J Therm Anal Calorim (2010) 102:1001–1010
DOI 10.1007/s10973-010-0890-x

Novel Mn(III) heterochelates: synthesis, thermal, spectroscopic, and coordination aspects

C. K. Modi · D. H. Jani

Received: 10 March 2010 / Accepted: 14 May 2010 / Published online: 4 June 2010

Abstract This article describes the synthesis, structural features, and thermal studies of novel Mn(III) heterochelates of the type $[Mn(SB_n)(L)(H_2O)]\cdot xH_2O$ [H_2SB_n = Nicotinic acid [1-(3-methyl-5-oxo-1-phenyl-4,5 dihydro-1H-pyrazol-4yl)-acylidene]-hydrazide where acyl = acetyl (H_2SB_1); benzoyl (H_2SB_2); propionyl (H_2SB_3); buteryl (H_2SB_4); phenyl acetyl (H_2SB_5); and HL = 5-Chloro-7-iodo-8-hydroxyquinoline (clioquinol)]. The heterochelates have been characterized on the basis of elemental analyses, magnetic susceptibility measurements, cyclic voltammetric studies, (FTIR and electronic) spectra, and thermal studies. The FAB mass spectrum of $[Mn(SB_1)(L)H_2O]\cdot 3H_2O$ has been carried out. The cyclic voltammetric studies reveal that quasi-reversible reduction process of Mn(III)/Mn(II) coupled system suggesting that the ligands readily destabilize higher oxidation states of metal ion. Kinetic parameters such as order of reaction (n) and the energy of activation (Ea) were calculated using Freeman–Carroll method. The pre-exponential factor (A), the activation entropy (S^*), the activation enthalpy (H^*), and the free energy of activation (G^*) were calculated using Horowitz–Metzger equations.

Keywords Mn(III) heterochelates · Schiff bases (H_2SB_n) · Clioquinol (HL) · Spectral studies · TG/DTG and DSC studies

C. K. Modi (✉)
Department of Chemistry, Bhavnagar University, Bhavnagar, Gujarat 364 002, India
e-mail: chetank.modi1@gmail.com

D. H. Jani
Department of Chemistry, Sardar Patel University, Vallabh Vidyanagar, Gujarat 388 120, India

Introduction

The chemistry of heterochelates of transition metals involving multidentate Schiff bases and bidentate uninegative ligands is gaining increasing popularity because of their ability to mimic the transamination reactions of biological importance. Manganese often plays an important role in numerous biological processes associated with utilization or generation of hydrogen peroxide or dioxygen. At least five functions of these types are known: manganese superoxide dismutase [1], manganese catalase [2], manganese peroxidase [3, 4], manganese ribonucleotide reductase [5], and oxygen evolving complex in photosystem-II [6, 7].

The report that 5-chloro-7-iodo-8-hydroxyquinoline (clioquinol, HL) attenuated Alzheimer's disease (AD) symptoms in human clinical trials [8] incited renewed interest in its pharmacodynamics, linking its possible beneficial therapeutical action to the chelation of transition metal ion in the brain. Recent reports indicate that clioquinol also mitigates neuropathological symptoms of Huntington's disease in a mouse model of this disorder [9]; clioquinol treatment decreased the accumulation of huntingtin aggregates, suggesting commonalities in the etiology of both neurological pathologies. These results suggest a broader clinical potential of clioquinol in the treatment of neurodegenerative diseases.

Nowadays, thermal analysis techniques (TG/DTG, DTA, DSC etc.) play an important role in studying the thermal behavior of metal complexes [10–14]. Thermogravimetry (TG) is a process in which a substance is decomposed in the presence of heat, which causes bonds in the molecules to be broken [15, 16]. The thermal behaviors of mixed-ligand complexes involving pyrazolone derivatives have been reported elsewhere [17, 18]. Pyrazolone-

based Schiff bases are less extensive. Our laboratory has been exploring the chemistry of this class of ligand [19–22]. During the course of our research, we have previously synthesized Mn(III) Schiff-base complexes involving heterocyclic β-diketone and diethylene triamine [23]. In continuation of our previous study, in this article, we describe synthetic, thermal, spectroscopic, and coordination aspects of some novel Mn(III) heterochelates with 4-acyl pyrazolone-based Schiff bases (H_2SB_n) (where $n = 1$–5) and 5-chloro-7-iodo-8-hydroxyquinoline (clioquinol) based drug.

Experimental

Materials

All the chemicals used were of analytical grade and used without further purification. The compounds, 1-phenyl-3-methyl-2-pyrazoline-5-ol and β-picolinic acid hydrazide, were purchased from E. Merck Ltd. (India). Acyl chlorides were purchased from Qualigens Fine Chemicals, India and used without further purification. 5-Chloro-7-iodo-8-hydroxyquinoline (clioquinol) was purchased from Bayer AG (Wuppertal, Germany).

Instruments

A model 5000/2960 SDT (TA Instruments, USA) was used to record simultaneous TG and DTG curves. The experiments were performed in N_2 atmosphere with a heating rate of 10 °C min^{-1} from room temperature to 700 °C in Al_2O_3 crucible. The samples sizes had masses ranging from 4 to 9.5 mg. The DTG sensitivity setting was a 0.05 mg s^{-1}. DSCs were recorded using DSC 2920 (TA Instrument, USA). The DSC curves were obtained at a heating rate of 10 °C min^{-1} in N_2 atmosphere over the temperature range of 50–400 °C, using aluminum crucible. FT-IR spectra (4,000–400 cm^{-1}) were recorded on Nicolet-400D spectrophotometer using KBr pellets. The magnetic moments were obtained by the Gouy's method using mercury tetrathiocyanato cobaltate (II) as a calibrant ($\chi_g = 16.44 \times 10^{-6}$ c.g.s. units at 20 °C). Diamagnetic corrections were made using Pascal's constant. Electronic spectra were recorded on a Shimadzu 160A UV-visible spectrophotometer using DMF as the solvent blank. The FAB mass spectrum of the heterochelate was recorded at SAIF, CDRI, Lucknow with JEOL SX-102/DA-6000 mass spectrometer. Cyclic voltammetric studies were performed using VA-Computrace No. 797, Metrohm with a HMDE (working), saturated Calomel (reference), and Platinum (counter) electrodes at the Department of Chemistry, Bhavnagar University, Bhavnagar. Solutions ($\sim 10^{-3}$ M) were prepared in DMF with 0.1 M tetrabutyl ammonium perchlorate as supporting electrolyte.

Synthesis of Schiff base ligands (H_2SB_n) (where $n = 1$–5)

The Schiff base ligands (H_2SB_n) (where $n = 1$–5) were synthesized according to the procedure described in the literature [21].

Synthesis of heterochelates

The preparation of heterochelates was carried out by mixing hot methanolic solution (25 mL) of $Mn(OAc)_3 \cdot 2H_2O$ (5 mmol) and a hot methanolic solution (25 mL) of the Schiff base (H_2SB_n) (5 mmol) and HL ligand (5 mmol) in water. The pH was adjusted to 6–7 by dropwise addition of 25% NaOH solution in water. The mixture was heated in a water bath for 3 h at 70 °C. The mixture was kept overnight at room temperature. The colored crystals obtained were washed with water, methanol, and finally with diethyl ether and dried in air.

Results and discussion

The analytical and physical data of the Schiff base ligands and their heterochelates are presented in Table 1. The heterochelates are colored and stable in air for extended period of time. They are sparingly soluble in water and in most organic solvents but completely soluble in DMF. When treated with KI, iodine was liberated. This is an indirect indication of Mn being in +3 oxidation state which is further supported by the solid state magnetic moments (Table 1).

IR spectra

In order to study the binding mode of Schiff bases (H_2SB_n) to the manganese ion in the heterochelates, the IR spectra of Schiff bases were compared with the spectra of the corresponding heterochelates. The Schiff base ligands in this investigation exhibit a broad band centered at 3,372–3,395 cm^{-1}. This indicates the involvement of the 5-OH group in intramolecular hydrogen bonding [13, 18, 24, 25] with the lone pair of azomethine nitrogen. It also suggests that the ligands exist in enol form in the solid state.

The Schiff base ligands (H_2SB_n) contain five potential donor sites: (i) the enolic oxygen of the 5-OH group; (ii) the cyclic azomethine nitrogen; (iii) the acyclic azomethine nitrogen; (iv) amide nitrogen of amide-imidol form of hydrazone moiety; and (v) carbonyl oxygen of amide-imidol form of hydrazone moiety.

Table 1 Physical, analytic, and electronic spectral data of ligands (H_2SB_n) and their heterochelates

Sr. no.	Compounds	M. wt./g mol^{-1}	Color	M.p./°C	Found (Calc.)/%				Electronic spectral data/cm^{-1}		μ_{eff}/B.M.
					C	H	N	M	*d–d* transition	ILCT transition	
1	H_2SB_1, $C_{18}H_{17}N_5O_2$	335.34	Light yellow	214	68.17 (68.26)	5.76 (5.39)	17.10 (16.77)	–	–	32534 (3.77)[a]	–
2	H_2SB_2, $C_{23}H_{19}N_5O_2$	397.41	Yellow	188	70.04 (69.44)	4.80 (4.78)	17.52 (17.61)	–	–	32577 (3.86)	–
3	H_2SB_3, $C_{19}H_{19}N_5O_2$	349.37	Light yellow	204	64.78 (65.32)	5.31 (5.48)	19.99 (20.04)	–	–	32556 (3.82)	–
4	H_2SB_4, $C_{20}H_{21}N_5O_2$	363.40	Orange	176	66.08 (66.10)	4.87 (5.82)	18.21 (19.27)	–	–	32552 (3.94)	–
5	H_2SB_5, $C_{24}H_{21}N_5O_2$	411.44	Orange	195	69.99 (70.06)	5.10 (5.14)	16.99 (17.02)	–	–	32589 (3.73)	–
6	$[Mn(SB_1)(L)(H_2O)]\cdot 3H_2O$ $C_{27}H_{27}ClIMnN_6O_7$	764.79	Reddish brown	310	42.38 (42.40)	3.55 (3.56)	10.95 (10.99)	7.16 (7.18)	18364 (2.82) 15692 (2.17) 14666 (1.76)	32380 (3.74)	4.81
7	$[Mn(SB_2)(L)(H_2O)]\cdot H_2O$ $C_{32}H_{25}ClIMnN_6O_5$	790.86	Reddish brown	323	48.59 (48.60)	3.16 (3.19)	10.62 (10.63)	6.93 (6.95)	20323 (2.93) 16712 (2.26)	32405 (3.79)	4.86
8	$[Mn(SB_3)(L)(H_2O)]\cdot H_2O$ $C_{28}H_{25}ClIMnN_6O_5$	742.82	Dull brown	327	45.25 (45.27)	3.37 (3.39)	11.30 (11.31)	7.39 (7.40)	18357 (2.89) 16767 (2.10) 14650 (1.93)	32435 (3.86)	4.93
9	$[Mn(SB_4)(L)(H_2O)]\cdot 2H_2O$ $C_{29}H_{29}ClIMnN_6O_6$	774.84	Dark brown	303	44.93 (44.95)	3.76 (3.77)	10.84 (10.85)	7.06 (7.09)	20302 (2.82) 16780 (2.09) 14652 (1.78)	32384 (3.72)	4.56
10	$[Mn(SB_5)(L)(H_2O)]\cdot H_2O$ $C_{33}H_{27}ClIMnN_6O_5$	804.88	Reddish brown	315	49.23 (49.24)	3.37 (3.38)	10.41 (10.44)	6.82 (6.83)	18350 (2.85) 16720 (2.30)	32389 (3.77)	4.74

[a] ($\log\varepsilon$) values in mol^{-1} cm^{-1}

The Schiff base ligands (H_2SB_n) show a sharp and strong band due to ν(C=N) of the acyclic azomethine group at 1,630–1,640 cm^{-1}. The observed low-energy shift of this band in the heterochelates and appearing at 1,614–1,622 cm^{-1} suggests the coordination of the azomethine nitrogen [26, 27].

The ν(N–H) and ν(C=O) modes of the lateral chain in the uncoordinated Schiff bases appearing at 3,170–3,192 and 1,690–1,702 cm^{-1}, respectively, indicates that the ligands exist in keto form in solid state. However, in solution, ligands probably exist in tautomeric enol form. The IR spectra of heterochelates show a considerable negative shift of 15–20 cm^{-1} in ν(C=O) absorption of the pyrazolone group, indicating a decrease in the stretching force constant of (C=O) as a consequence of coordination through the oxygen atom of the ligand. Meanwhile, the new absorption bands attributed to ν(C–O) [28] was observed at 1,343–1,352 cm^{-1}. From these observations, it is concluded that the ligand reacts in enol form with prototropy, which incorporates into proton transfer through oxygen atom of the ligand forming two bonds with the metal ion.

In the heterochelates investigated, the bands observed in the region 3452–3467, 1265–1278, 820–834, and 677–704 cm^{-1} are attributed to –OH stretching, bending, rocking, and wagging vibrations, respectively, due to the presence of water molecules. The presence of rocking band indicates the coordination nature of the water molecule [29].

A comparison of the main IR frequencies of Mn(III) heterochelates with that of clioquinol (HL) ligand showed the following results. Two absorption peaks in the spectrum of the ligand due to ν(O–H) and ν(C=N) cyclic azomethine groups were observed at 3,420 and 1,605 cm^{-1}, respectively. The absence of the former band in the spectra of the heterochelates suggests that this moiety participated in the bonding to the metal ion. The latter band corresponding to ν(C=N) shifted to the lower frequency region ($\sim$1,592 cm^{-1}) in the spectra of the heterochelates. Accordingly, clioquinol (HL) ligand, in the isolated heterochelates, appears to act as a uninegative bidentate ligand through the nitrogen atom of the cyclic azomethine group and enolic oxygen of the hydroxyl group by deprotonation.

In the far-IR region, two new bands at 448–462 and 415–422 cm^{-1} in the heterochelates are assigned to ν(M–O) and ν(M–N) modes, respectively. All of these data confirm the fact that H_2SB_n behaves as a dinegative tridentate ligand forming a conjugated chelate ring, with the ligand existing in the heterochelates in the enolized form.

Mass spectra

The recorded mass spectra and the molecular ion peak for the heterochelate $[Mn(SB_1)(L)H_2O]\cdot 3H_2O$ have been used to confirm the molecular formulae. The mass spectrum of

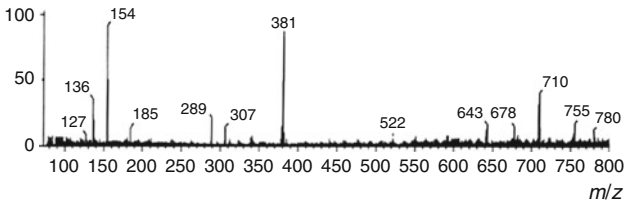

Fig. 1 The typical FAB-mass spectrum of a heterochelate $[Mn(SB_1)(L)H_2O]\cdot 3H_2O$

$[Mn(SB_1)(L)H_2O]\cdot 3H_2O$ shows a large number of peaks corresponding to the successive degradation of the molecule as shown in Fig. 1, and its fragmentation pattern is given in Scheme 1. The first peak at *m/e* 710 represents the molecular ion peak of the heterochelate. The primary fragmentation of the heterochelate takes place due to the loss of $-CH_3$ group and one coordinated water molecule from the species (a) to give species (b) with peak at *m/e* 678. The sharp peak (base peak) observed at *m/e* 381 represents the stable species (e) with 99.6% abundance.

Electronic spectra and magnetic moments

The information regarding geometry of the heterochelates was obtained from their electronic spectral data and magnetic moment values. The magnetic moment values of Mn(III) heterochelates were in the range of 4.56–4.93 B.M. [23, 30]. The electronic spectral data along with molar extinction coefficient (logε) values of the free ligands (H_2SB_n) (where $n = 1$–5) and their heterochelates are presented in Table 1. The electronic spectra of free ligands showed an intense band at $\sim$32,500 cm^{-1}. The high intensity of this band may be due to $\pi \rightarrow \pi^*$ intra-ligand charge transfer transition (ILCT). In this study, electronic spectra of Mn(III) heterochelates yielded one charge transfer band and multiple *d–d* transitions. The heterochelates investigated here are all six coordinated; therefore, either octahedral or distorted octahedral geometry around the metal ion is expected. The appearance of two/three bands in the heterochelates studied suggests that they possess distorted octahedral structures. Such distortion is most probably due to Jahn–Teller's effect as well as due to steric effect of the bulky ligands. Keeping in view the distorted octahedral structures, the band observed at $\sim$18,350 cm^{-1} for 6, 8, and 10 and 20,300 cm^{-1} for 7 and 10 compounds can be assigned to $^5B_{1g} \rightarrow {}^5E_g$ transition. Similarly, the second shoulder observed near 15,650–16,780 cm^{-1} can be assigned to $^5B_{1g} \rightarrow {}^5B_{2g}$ transition. The third band observed near 14,650 cm^{-1} for 6, 8, and 9 is assigned to $^5B_{1g} \rightarrow {}^5A_{2g}$ transition. This band is not seen in the remaining heterochelates. This may be due to low energy of this transition and greater absorption in the UV part of the spectra (highly intense charge transfer transition). The highly intense band

Scheme 1 The suggested fragmentation pattern of $[Mn(SB_1)(L)H_2O]\cdot 3H_2O$

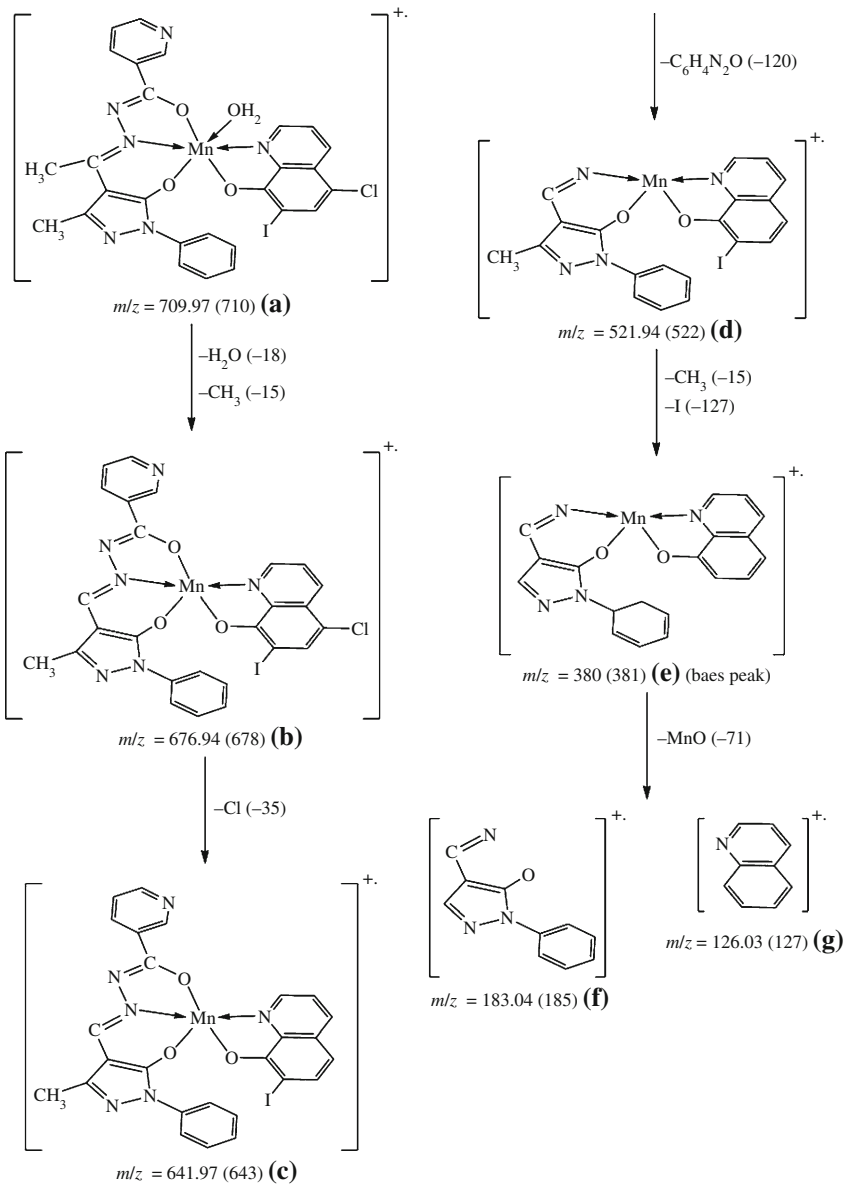

observed near 32,380 cm^{-1}, which may be due to $\pi \rightarrow \pi^*$ ILCT of the azomethine group. From the magnetic measurement and electronic spectral data, a six-coordinated distorted octahedral stereochemistry is proposed for all the heterochelates.

Cyclic voltammetric studies

The redox behaviour of heterochelates was studied at a slow scan rate of 0.05 V s^{-1} over a potential range from −0.2 to −1.75 V. The typical cyclic voltammogram of $[Mn(SB_3)(L)H_2O]\cdot H_2O$ (Fig. 2) shows quasi-reversible reduction process in the range from −0.35 to −0.55 V assignable to the reduction of Mn(III)/Mn(II)-coupled system suggesting that the ligands readily destabilize higher oxidation states of manganese. The electrochemical

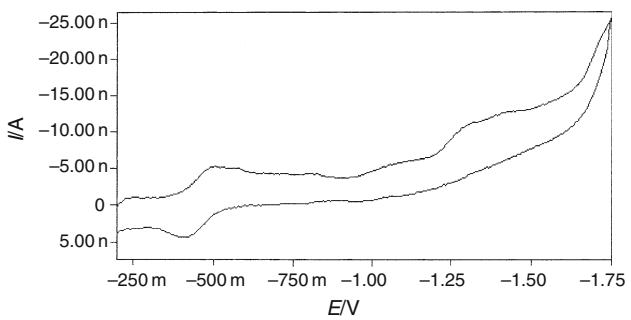

Fig. 2 The typical cyclic voltammogram of a heterochelate $[Mn(SB_3)(L)H_2O]\cdot H_2O$ at 0.05 V s^{-1} scan rate

stabilization of Mn(II) oxidation level is basically due to the presence of one additional basic oxyanion per manganese, providing another negative charge to the metal ion.

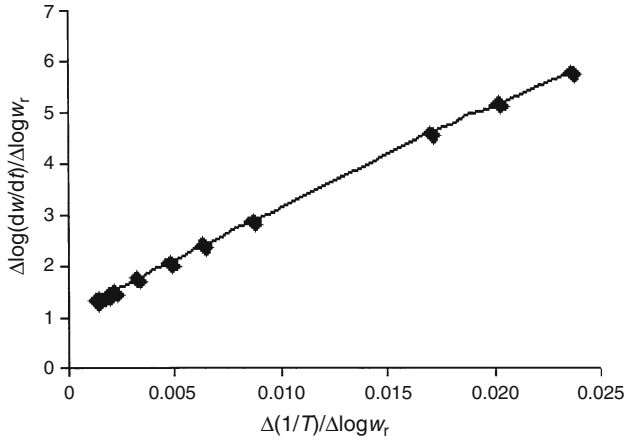

Fig. 3 The typical Freeman–Carroll plot for thermal degradation of a heterochelate $[Mn(SB_3)(L)H_2O]\cdot H_2O$

The second redox wave observed at −1.41 V is attributed as due to the reduction of Mn(II) to Mn(0), which is irreversible in the nature.

Calculation of activation thermodynamic parameters of the decomposed heterochelates

Each decomposition process follows:

$$\text{Solid-1} \longrightarrow \text{heat Solid-2} + \text{gas}$$

This process comprises several stages. The method reported by Freeman–Carroll method [31] has been adopted. A typical curve of $[\Delta\log(dw/dt)/\Delta\log w_r]$ versus $[\Delta(1/T)/\Delta\log w_r]$ for the heterochelate $[Mn(SB_3)(L)H_2O]\cdot H_2O$ is shown in Fig. 3. The slope of the plot gave the value of $E_a/2.303\ R$ and the order of reaction (n) was determined from the intercept.

The thermal behavior of the prepared heterochelates

In the following paragraphs, the thermal behavior of the synthesized heterochelates, characterized on the basis of TG/DTG and DSC methods, is described. Thermal data and kinetic parameters of the heterochelates are given in Tables 2 and 3, respectively.

$[Mn(SB_3)(L)H_2O]\cdot H_2O$

TG/DTG and DSC curves of the heterochelate $[Mn(SB_3)(L)(H_2O)]\cdot H_2O$ are represented in Figs. 4 and 5, respectively. The thermal decomposition of the heterochelate $[Mn(SB_3)(L)(H_2O)]\cdot H_2O$ takes place in three stages. The thermal dehydration of this heterochelate takes place in a single step between 40 and 190 °C, with a mass loss of 4.75% (calc. 4.84%). The maximum rate of mass loss is indicated by the DTG peak at 152 °C. One mole of lattice and one mole of coordinated water molecules are removed in this stage of dehydration. This process is accompanied by endothermic effect at 120 °C in DSC curve. The total loss of two water molecules is a first-order reaction and the value of the energy of activation for the dehydration process is 3.16 kJ mol^{-1}. The second stage, which occurs in the temperature range of 190–360 °C with a DTG peak observed at 310 °C, corresponds to the decomposition of the HL ligand. The observed mass loss is 40.67%, which is consistent with the theoretical value of 40.99%. The endothermic peak at 324 °C corresponds to this stage is given by DSC curve. The third stage is related to the decomposition of H_2SB_3 ligand in the temperature range of 360–700 °C with two well-separated DTG peaks at 409 and 612 °C, accompanied by a mass loss of 44.92% (calc. 44.60%). The overall mass loss observed is 90.34% as compared to the theoretical value (90.43%). The end product estimated as MnO, has the observed mass of 9.49% compared to the calculated value of 9.55%.

$[Mn(SB_1)(L)H_2O]\cdot 3H_2O$

The $[Mn(SB_1)(L)H_2O]\cdot 3H_2O$ heterochelate undergoes decomposition in three stages. The thermal dehydration of this heterochelate takes place in a single step between 50 and 225 °C, with a mass loss of 9.67% (calc. 9.41%). The maximum rate of mass loss is indicated by the DTG 182 °C. Three moles of lattice and one mole of coordinated water molecules are removed in this stage of dehydration. This process is accompanied by two endothermic effects at 143 and 174 °C in DSC curve [32]. The total loss of three moles of lattice and one mole of coordinated water molecules is a first-order reaction and the value of energy of activation for the dehydration process is 12.28 kJ mol^{-1}. The second stage occurs in the temperature range 225–410 °C, with the mass loss (39.40%) is due to the removal of HL ligand from the heterochelate (calc. 39.81%). The DTG peak corresponding to this stage is found at 348 °C. This process is further supported by an exothermic process at 269 °C in DSC curve. The third stage is related to the decomposition of H_2SB_1 ligand, taking place in the temperature range 410–700 °C with a DTG peak at 526 °C and being accompanied by a mass loss of 41.78% (calc. 41.49%). The overall mass losses are observed to be 90.85%, which is in very good agreement with the calculated value of 90.71%. The final residue, estimated as MnO has the observed mass 9.12% as against the calculated value of 9.27%.

$[Mn(SB_2)(L)H_2O]\cdot H_2O$

The thermal decomposition of the heterochelate $[Mn(SB_2)(L)H_2O]\cdot H_2O$ takes place in three stages. Two endothermic

Table 2 Thermoanalytic results (TG/DTG and DSC) of heterochelates

Heterochelates	TG range/°C	DTG_{max}/°C	DSC_{max}/°C	Mass loss/% obs. (calc.)	Assignment
$[Mn(SB_1)(L)(H_2O)]\cdot 3H_2O$	50–225	182	143, 174 (+)	9.67 (9.41)	Loss of three lattice + one coordinated water molecules
	225–440	348	269 (+)	39.40 (39.81)	Removal of one mole of HL ligand
	410–700	526	–	41.78 (41.49)	Removal of one mole of H_2SB_1 ligand leaving MnO residue
				90.85[a] (90.71)	
$[Mn(SB_2)(L)(H_2O)]\cdot H_2O$	50–215	–	129, 153 (+)	4.53 (4.54)	Loss of one lattice + one coordinated water molecules
	215–460	336	251 (−)	38.45 (38.50)	Removal of one mole of HL ligand
	460–700	624	–	48.08 (48.22)	Removal of one mole of H_2SB_2 ligand leaving MnO residue
				91.06[a] (91.26)	
$[Mn(SB_3)(L)(H_2O)]\cdot H_2O$	40–190	152	120 (+)	4.75 (4.84)	Loss of one lattice + one coordinated water molecules
	190–360	310	324 (+)	40.67 (40.99)	Removal of one mole of HL ligand
	360–700	409, 612	–	44.92 (44.60)	Removal of one mole of H_2SB_3 ligand leaving MnO residue
				90.34[a] (90.43)	
$[Mn(SB_4)(L)(H_2O)]\cdot 2H_2O$	50–130	–	–	4.53 (4.64)	Loss of two lattice water molecules
	130–220	179	144 (+)	2.28 (2.32)	Loss of one coordinated water molecule
	220–390	294	243 (−)	39.03 (39.29)	Removal of one mole of HL ligand
	390–700	445	–	44.78 (44.57)	Removal of one mole of H_2SB_4 ligand leaving MnO residue
				90.62[a] (90.82)	
$[Mn(SB_5)(L)(H_2O)]\cdot H_2O$	50–115	–	138 (+)	2.20 (2.23)	Loss of one lattice water molecule
	115–220	174	188 (+)	2.21 (2.23)	Loss of one coordinated water molecule
	220–400	253	286 (+)	37.45 (37.83)	Removal of one mole of HL ligand
	400–700	478	–	49.09 (48.88)	Removal of one mole of H_2SB_5 ligand leaving MnO residue
				90.95[a] (91.17)	

(+) Endothermic; (−) exothermic

[a] Total mass loss

peaks (DSC) were observed at 129 and 153 °C, in the temperature range of 50–215 °C with the mass loss (obs. 4.53%; calc. 4.54%), which correspond to the loss of one water molecule coordinated to the Mn(III) and the one lattice water molecule present in the heterochelate, respectively. It was found that the loss of two water molecules is a first-order reaction, and the value of the energy of activation for the dehydration process is 5.25 kJ mol^{-1}. After dehydration, the crystal structure of the heterochelate is distorted. In the second stage between 215 and 460 °C, the HL ligand degrades as one maximum in the DTG curve at 336 °C with a mass loss of 38.45% (calc. 38.50%). It is accompanied by an exothermic process at 251 °C in the DSC curve. The third stage, which occurs in the temperature range of 460–700 °C with DTG peak observed at 624 °C, corresponds to the decomposition of H_2SB_2 ligand. The observed mass loss (48.08%) is coinciding with the calculated value of 48.22%. The overall mass losses are observed to be 91.06%, which is in very good agreement with the calculated value of 91.26%. The final residue, estimated as MnO, has the observed mass 8.67% as against the calculated value of 8.90%.

$[Mn(SB_4)(L)H_2O]\cdot 2H_2O$

The thermal decomposition of the heterochelate $[Mn(SB_4)(L)H_2O]\cdot 2H_2O$ takes place in four stages. The first stage is related to the liberation of two crystalline water molecules from the heterochelate in the temperature range of 50–130 °C, accompanied by a mass loss of 4.53% (calc. 4.64%). Two moles of lattice water molecules are removed in this stage of dehydration. The loss of one lattice water molecule is a first-order reaction, and the value of the energy of activation for the dehydration process is

Table 3 Kinetic parameters of heterochelates

Heterochelates	TG range/°C	E_a/kJ mol^{-1}	n	A/s^{-1}	S*/J K^{-1} mol^{-1}	H*/kJ mol^{-1}	G*/kJ mol^{-1}
$[Mn(SB_1)(L)(H_2O)]\cdot 3H_2O$	50–225	12.28	0.99	0.95	−100.75	9.65	40.36
	225–410	15.25	0.99	5.32	−101.32	9.75	63.33
	410–700	20.29	1.00	9.85	−95.55	17.20	95.59
$[Mn(SB_2)(L)(H_2O)]\cdot H_2O$	50–215	5.25	0.98	0.17	−101.09	0.88	29.57
	215–460	24.28	1.00	3.34	−96.98	22.31	65.55
	460–700	42.19	1.00	5.81	−97.13	30.37	107.67
$[Mn(SB_3)(L)(H_2O)]\cdot H_2O$	40–190	3.16	1.00	0.01	−102.23	0.43	41.51
	190–360	12.67	1.00	0.48	−101.25	4.49	67.35
	360–700	22.25	0.99	31.55	−95.54	22.36	98.11
$[Mn(SB_4)(L)(H_2O)]\cdot 2H_2O$	50–130	3.01	1.01	0.10	−101.99	0.33	31.44
	130–220	26.66	0.98	0.15	−101.35	2.26	55.55
	220–390	32.99	1.01	8.40	−95.21	25.39	105.44
	390–700	38.78	0.99	13.51	−94.45	34.64	109.98
$[Mn(SB_5)(L)(H_2O)]\cdot H_2O$	50–115	4.01	1.00	0.10	−101.55	0.37	32.33
	115–220	17.79	0.98	2.20	−97.56	12.15	61.65
	220–400	31.55	1.01	33.55	−94.44	21.44	75.57
	400–700	42.44	0.99	156.2	−93.23	33.53	92.54

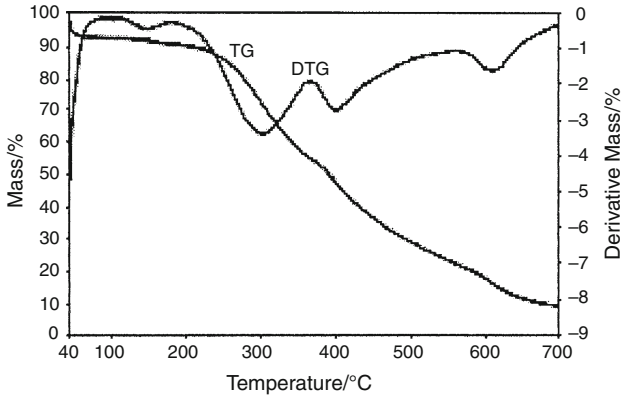

Fig. 4 TG/DTG curves of the heterochelate $[Mn(SB_3)(L)H_2O]\cdot H_2O$

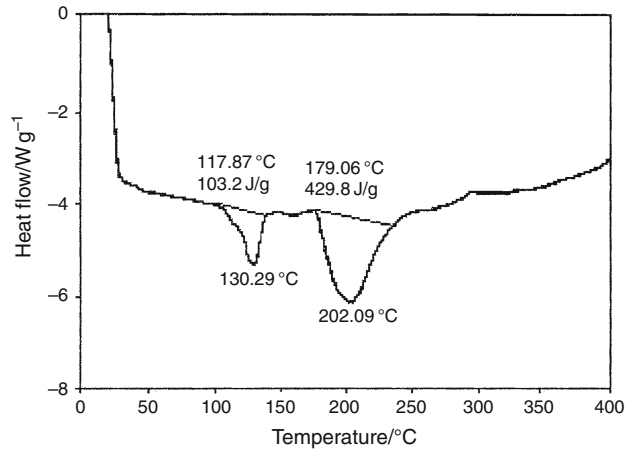

Fig. 5 DSC curve of the heterochelate $[Mn(SB_3)(L)H_2O]\cdot H_2O$

3.01 kJ mol^{-1}. The second stage is related to the liberation of one coordinated water molecule from the heterochelate in the temperature range of 130–220 °C, accompanied by a mass loss of 2.28% (calc. 2.32%). The maximum rate of mass loss is indicated by the DTG peak at 179 °C. This process is accompanied by an endothermic effect at 144 °C in DSC curve. On heating, the decompositions of ligands occurred. In the third stage between 220 and 390 °C, the HL ligand degrades as one maximum in the DTG curve at 294 °C with a mass loss 39.03% (calc. 39.29%). It is accompanied by an exothermic process at 243 °C in the DSC curve. The fourth stage, which occurs in the temperature range 390–700 °C with DTG peak observed at 445 °C, corresponds to the decomposition of H_2SB_4 ligand molecule. The observed mass loss (44.78%) is coinciding with the calculated value of 44.57%. The overall mass loss observed has a value of 90.62% as against the theoretical value (90.82%). The final residue, estimated as MnO, has the observed mass of 9.29% as against the calculated value of 9.15%.

$[Mn(SB_5)(L)H_2O]\cdot H_2O$

The heterochelate $[Mn(SB_5)(L)H_2O]\cdot H_2O$ undergoes thermal decomposition in four stages. The first stage is related to the liberation of one crystalline water molecule from the heterochelate in the temperature range of 50–115 °C, accompanied by a mass loss of 2.20% (calc. 2.23%). This process is supported by an endothermic effect at 138 °C in DSC curve. The loss of one lattice water molecule is a first-order reaction, and the value of the energy of activation for

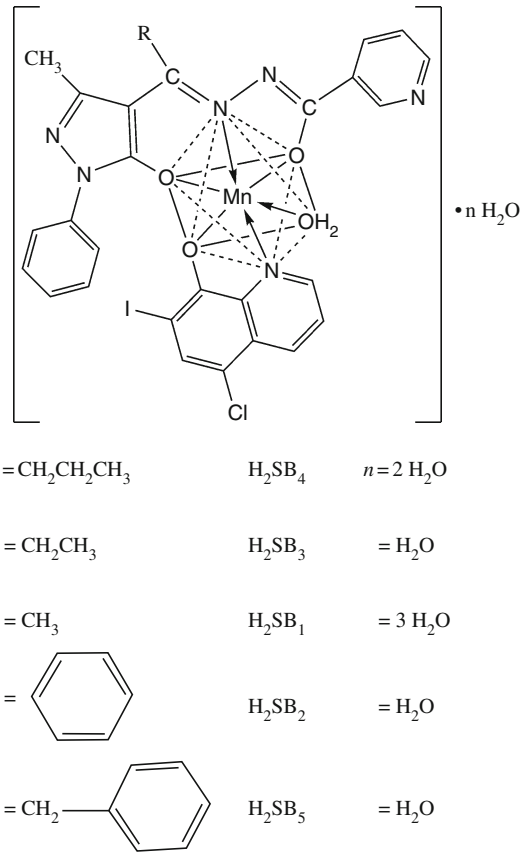

Fig. 6 The suggested structure of heterochelates

the dehydration process is 4.01 kJ mol^{-1}. The second stage occurs in the temperature range 115–220 °C, with the mass loss of 2.21% (calc. 2.23%) being due to the removal of one coordinated water molecule from the heterochelate. The DTG peak corresponding to this stage is found at 174 °C. This process is further supported by an endothermic peak at 188 °C in DSC curve. On heating, decompositions of ligands occurred. The third (from 220 to 400 °C) and fourth (from 400 to 700 °C) stages may be due to the decomposition of HL and H_2SB_5 ligand molecules, respectively. The observed mass losses for these temperature ranges are 37.45 and 49.09%, respectively. The overall mass losses are observed to be 90.95%, which is in very good agreement with the calculated value of 91.17%. The final residue, estimated as MnO, has the observed mass 8.72% as against the calculated value of 8.81%.

Non-isothermal calculations were used extensively to evaluate kinetic parameters (Table 3) for the different thermal decomposition steps in the heterochelates employing the Horowitz–Metzger equations [33]. The results of activation enthalpy ($H^*=E_a - RT_s$); the activation entropy ($S^* = 2.303[\log Ah/KT]R$); the pre-exponential factor ($E_a/RT_s^2 = A/\exp[-E_a/RT_s]$), and the free energy of activation ($G^* = \Delta H^* - T_sS^*$) where A, T_s, K, and h are the pre-exponential factor, heating rate, peak temperature, Boltzman and Plank constants, respectively. There was no definite trend in the values of the entropy of activation. However, the negative value of the entropy of activation indicated that the activated complex has a more ordered structure than the reactants, and the reactions are slower than normal [34–36]. The kinetic parameters, especially the energy of activation (*E*a) values, are helpful in assigning the strength of heterochelates [37]. The calculated *E*a values of the investigated heterochelates for the first dehydration step were in the range of 3.01–12.28 kJ mol^{-1} (Table 3). Based on the *E*a values, the thermal stabilities of heterochelates in the decreasing order are

$$[Mn(SB_1)(L)(H_2O)]\cdot 3H_2O > [Mn(SB_2)(L)(H_2O)]\cdot H_2O > [Mn(SB_5)(L)(H_2O)]\cdot H_2O > [Mn(SB_3)(L)(H_2O)]\cdot H_2O > [Mn(SB_4)(L)(H_2O)]\cdot 2H_2O$$

From the above discussion, an octahedral structure of the heterochelates can tentatively be assumed as shown in Fig. 6.

Acknowledgements We wish to express our gratitude to the Department of Chemistry, Sardar Patel University, Vallabh Vidyanagar, Gujarat, India for providing the necessary laboratory facilities.

References

1. Ludvig ML, Patridge KA, Stallings WC. Manganese in metabolism and enzyme function. London: Academic press; 1986. p. 405–30.
2. Brudvig GW, Crabtree RH. Bioinorganic chemistry of manganese related to photosynthetic oxygen evolution. Prog Inorg Chem. 1989;37:99–142.
3. Wariishi H, Akileswaran L, Gold MH. Manganese peroxidase from the basidiomycete *Phanerochaete chrysosporium*: spectral characterization of the oxidized states and the catalytic cycle. Biochemistry. 1988;27:5365–70.
4. Glenn JK, Akileswaran L, Gold MH. Mn(II) oxidation is the principal function of the extracellular Mn-peroxidase from *Phanerochaete chrysosporium*. Arch Biochem Biophys. 1986; 251:688–96.
5. Willing A, Follmann H, Auling G. Ribonucleotide reductase of *Brevibacterium ammoniagenes* is a manganese enzyme. Eur J Biochem. 1988;170:603–11.
6. Debus R. The manganese and calcium ions of photosynthetic oxygen evolution. Biochim Biophys Acta (Bioenerg). 1992;1102: 269–352.
7. Kirk ML, Lab MS, Hatfield S, Pecararo VL. Structurally diverse manganese(III) Schiff base complexes: chains, dimers, and cages. Inorg Chem. 1989;28:2037–44.
8. Ritchie CW, Bush AI, Mackinnon A, Macfarlane S, Mastwyk M, MacGregor L, Kiers L, Cherny R, Li QX, Tammer A, Carrington D, Mavros C, Volitakis I, Xilinas M, Ames D, Davis S, Beyreuther K, Tanzi RE, Masters CL. Metal-protein attenuation with iodochlorhydroxyquin (clioquinol) targeting a beta amyloid deposition and toxicity in Alzheimer disease: a pilot phase 2 clinical trial. Arch Neurol. 2003;60:1685–91.

9. Nguyen T, Hamby A, Massa SM. Clioquinol down-regulates mutant huntingtin expression in vitro and mitigates pathology in a Huntington's disease mouse model. Proc Natl Acad Sci USA. 2005;102:11840–5.
10. Icbudak H, Heren Z, Kose DA, Necefoglu H. Bis(nicotinamide) and bis(*N*,*N*-diethylnicotinamide) *p*-hydroxybenzoate complexes of Ni(II), Cu(II) and Zn(II): spectrothermal studies. J Therm Anal Calorim. 2004;76:837–51.
11. El-Boraey HA. Structural and thermal studies of some aroylhydrazone Schiff''s bases-transition metal complexes. J Therm Anal Calorim. 2005;81:339–46.
12. Bakalova A, Varbanov H, Buyukliev R, Momekov G, Ivanov D. Palladium(II) complexes with 5-methyl-5-(4-pyridyl)-2,4-imidazolidenedione. J Therm Anal Calorim. 2009;95(1):241–6.
13. Modi CK, Thaker BT. Some novel tetradentate Schiff base complexes VO(IV) and Cu(II) involving fluorinated heterocyclic β-diketones and polymethylene diamines of varying chain length. J Therm Anal Calorim. 2008;94(2):567–77.
14. Köse DA, Gökçe G, Gökçe S, Uzun İ. Bis(*N*,*N*-diethylnicotinamide) *p*-chlorobenzoate complexes of Ni(II), Zn(II) and Cd(II). J Therm Anal Calorim. 2009;95(1):247–51.
15. Albano CL, Sciamanna R, Aquino T, Martinez JJ (2000) European Congress on computational methods in applied sciences and engineering. ECOMAS 2000, Barcelona; Sept 2000. pp. 11–4.
16. Carrasco F. The evaluation of kinetic parameters from thermogravimetric data: comparison between established methods and the general analytical equation. Thermochim Acta. 1993;213: 115–34.
17. Xu GC, Zhang L, Liu L, Liu GF, Jia DZ. Thermal kinetic TG-analysis of the mixed-ligand copper(II) and nickel(II) complexes of N-(1-phenyl-3-methyl-4-benzylidene-5-pyrazolone) *p*-nitrobenzoylhydrazide and pyridine. Thermochim Acta. 2005; 429:31–42.
18. Surati KR, Thaker BT. Synthesis, spectroscopic and thermal investigation of Schiff-base complexes of Cu(II) derived from heterocyclic β-diketone and various primary amines. J Coord Chem. 2006;59:1191–202.
19. Modi CK, Patel MN. Synthetic, spectroscopic and thermal aspects of some heterochelates. J Therm Anal Calorim. 2008; 94(1):247–55.
20. Modi CK. Synthesis, spectral investigation and thermal aspects of coordination polymeric chain assemblies of some transition metal ions with bis-pyrazolones. Spectrochim Acta A. 2009;71:1741–8.
21. Modi CK, Jani DH, Patel HS, Pandya HM. Novel Fe(III) heterochelates: synthesis, structural features and fluorescence studies. Spectrochim Acta A. 2010;75(4):1321–8.
22. Jani DH, Patel HS, Keharia H, Modi CK. Novel drug-based Fe(III) heterochelates: synthetic, spectroscopic, thermal and in vitro antibacterial significance. Appl Organomet Chem. 2010;24(2): 99–111.
23. Modi CK, Patel IA, Thaker BT. Manganese(III) Schiff-base complexes involving heterocyclic β-diketone and diethylene triamine. J Coord Chem. 2008;61(19):3110–21.
24. Marchetti F, Pettinari C, Pettinari R, Cingolani A, Rossi M, Caruso F. Organotin(IV) derivatives of novel β-diketones Part V. Synthesis and characterization of di- and triorganotin(IV) derivatives of 4-acyl-5-pyrazolones modified in position 3 of the pyrazole. Crystal structure of (1,3-diphenyl-4-benzoyl-pyrazolon-5-ato)triphenyltin(IV). J Organomet Chem. 2002;645:134–45.
25. Marchetti F, Pettinari C, Pettinari R, Cingolani A, Leonesi D, Lorenzotti A. Group 12 metal complexes of tetradentate N_2O_2–Schiff-base ligands incorporating pyrazole synthesis, characterization and reactivity toward S-donors, N-donors, copper and tin acceptors. Polyhedron. 1999;18:3041–50.
26. Xu G, Liu L, Zhang L, Liu G, Jia D, Lang J. Synthesis and characterization of tetra-μ-phenolatotetrazinc(II) complex with 1-phenyl-3-methyl-4-(salicylidene hydrazone)-phenylethylene-pyrazolone-5. Struct Chem. 2005;16:431–8.
27. Modi CK, Thaker BT. Synthesis and characterization of lanthanide complexes of 1-phenyl-3-methyl-5-hydroxy-4-pyrazolylphenyl ketone-2′-picolinoyl hydrazone. Indian J Chem. 2002; 41A:2544–7.
28. Hu X, Zhang L, Liu L, Liu G, Jia D, Xu G. Synthesis and structural characterization of three hydrogen-bonding connected supramolecular complexes of nickel, zinc and copper with 1,3-diphenyl-4-(salicylidene hydrazide)-acetyl-pyrazolone-5 and 2,2′-bipyridine. Inorg Chim Acta. 2006;359:633–41.
29. Nakamoto K. Infrared spectra and Raman spectra of inorganic and coordination compounds, Part B: application in coordination, organometallic, and bioinorganic chemistry. 6th ed. New Jersey: Wiley; 2009.
30. Patel IA, Patel P, Goldsmith S, Thaker BT. Manganese (III) complexes with hexadentate Schiff bases derived from heterocyclic β-diketones and triethylene tetramine. Indian J Chem. 1999;38A:427–33.
31. Freeman ES, Carroll B. The application of thermoanalytical techniques to reaction kinetics: the thermogravimetric evaluation of the kinetics of the decomposition of calcium oxalate monohydrate. J Phys Chem. 1958;62:394–7.
32. House JE Jr, Bailar JC Jr. Solid state determination of tris(ethylenediamine)- and tris(propylenediamine) chromium complexes. J Inorg Nucl Chem. 1976;38:1791–3.
33. Horowitz HH, Metzger G. A new analysis of thermogravimetric traces. Anal Chem. 1963;35:1464–8.
34. Modi CK, Patel SH, Patel MN. Transition metal complexes with uninegative bidentate Schiff base synthetic, thermal, spectroscopic and coordination aspects. J Therm Anal Calorim. 2007;87(2):441–8.
35. Aravindakshan KK, Muraleedharan K. Thermal decomposition kinetics of 2-furaldehyde thiosemicarbazone complexes of cadmium(II) and mercury(II). Thermochim Acta. 1989;155:247–53.
36. Frost AA, Pearson RG. Kinetics and mechanism. New York: John Wiley; 1961.
37. Kharadi GJ, Patel KD. Antibacterial, spectral and thermal aspects of drug based-Cu(II) mixed ligand complexes. Appl Organomet Chem. 2009;23(10):391–7.